



## Oxygen vacancies confined in ultrathin nickel oxide nanosheets for enhanced electrocatalytic methanol oxidation



Wenlong Yang, Xianpeng Yang, Jun Jia, Changmin Hou, Hongtao Gao, Yaning Mao, Chao Wang, Jiehua Lin, Xiliang Luo\*

*Key Laboratory of Optic-electric Sensing and Analytical Chemistry for Life Science, MOE, Shandong Key Laboratory of Biochemical Analysis, College of Chemistry and Molecular Engineering, Qingdao University of Science and Technology, Qingdao 266042, China*

### ARTICLE INFO

**Keywords:**

Nickel oxide  
Ultrathin nanosheets  
Oxygen vacancy  
Electrocatalysis  
Methanol oxidation

### ABSTRACT

Owing to the relatively sluggish charge transport and reaction kinetics in nickel-based oxides, the electrocatalytic efficiency for methanol oxidation reaction (MOR) is still far below what is expected. Herein, ultrathin NiO nanosheets with abundant oxygen vacancies is put forward as an applicable catalytic model to get in-depth insights into the role that oxygen vacancies play in MOR process. Theoretical investigations reveal that the incorporation of oxygen vacancies can not only enhance the electrical conductivity of NiO crystals, but also reduce the adsorption energy of methanol molecules onto the active surface, both of which are more favorable for optimizing the overall electrocatalytic MOR performance. Thanks to the ultrathin two-dimensional (2D) features and remarkably modulated electronic structures, ultrathin NiO nanosheets with abundant oxygen vacancies exhibit a dramatically improved electrocatalytic activity for MOR, which is significantly higher than that of the sample with less oxygen vacancies and bulk NiO. This work opens a promising and feasible pathway for the design and synthesis of highly efficient non-noble MOR catalysts.

### 1. Introduction

As a promising and sustainable pathway to solve global environmental problems and energy issues, direct methanol fuel cells (DMFCs) have attracted much attention due to the high energy density, low operating temperature and low pollution emission [1–4]. Up to now, although previous studies have reported that Pt-based catalysts show the highest catalytic activity for methanol oxidation in both acidic and alkaline media, their scarce resource and high cost as well as the ease of poisoning effect during the methanol oxidation reaction (MOR) process tremendously limit their practical utilization [5–9]. To address this issue, many efforts have been devoted to developing efficient earth-abundant transition-metal oxides (TMOs) as alternative MOR electrocatalysts to noble metal counterparts for the commercialization of DMFCs [10–12]. Among these materials, Nickel-based oxides are considered as attractive electrocatalyst candidates because of their good surface oxidation properties and potential durability [13–16]. However, the electrocatalytic performance of these materials is still very low, mainly due to the low amount of active sites and poor electrical conductivity in the previously prepared catalysts. Therefore, it is of significance but challenging to fabricate Nickel-based oxides with

abundant active sites and enhanced electrical conductivity for achieving efficient MOR catalytic activity.

Recently, ultrathin two-dimensional (2D) nanosheets have drawn explosive attention because of their impressive surface structures and electronic properties, which may provide a favorable platform to realize the maximization of electrochemical performance [17,18]. In general, the ultra-high specific surface areas originated from their ultrathin 2D structures allow a large fraction of exposed surface atoms to act as active sites to improve the kinetics of catalytic reactions. Also, the ultrathin thickness is helpful to decrease the length of the diffusion paths, ensuring rapid interfacial electrons transport during the electrocatalytic process. It is interesting to note that more defective structures can be formed with the thickness of 2D nanosheets reduced to atomic scale, giving rise to a non-negligible influence on their electronic structures and physicochemical properties, which would bring tremendous opportunities to achieve significantly improved MOR performance. Inspired by this consideration, defect engineering, especially for oxygen vacancies ( $V_O$ ) has been considered as an effective strategy to optimize the number and reactivity of active sites as well as electrical conductivity of TMO materials, rendering them to be promising candidates for electrochemical applications [19,20]. In spite of many advantages

\* Corresponding author.

E-mail address: [xiliangluo@qust.edu.cn](mailto:xiliangluo@qust.edu.cn) (X. Luo).

derived from the defect engineering strategy in the electrocatalytic field, rare attention is paid to the effect of oxygen vacancies on MOR performance, and it is still an open question to gain in-depth understanding of the correlations between oxygen vacancies and intrinsic catalytic activity for MOR. Herein, by taking ultrathin NiO nanosheets with abundant oxygen vacancies as an example, we highlight the role of oxygen vacancies that played in the MOR process via a combination of experimental studies and theoretical calculations, with efforts to illuminate the efficacy of oxygen vacancies in promoting the electrocatalytic MOR performance.

## 2. Experimental section

### 2.1. Materials

All reagents were of analytical reagent grade, purchased from Sinopharm Chemical Reagent Co., Ltd., and used as received without further purification.

### 2.2. Preparation of ultrathin Ni-Based nanosheets precursors

The ultrathin Ni-based nanosheets precursors were synthesized using a modification of the method reported previously [21]. In a typical experiment, 0.12 g  $\text{NiCl}_2 \cdot 6\text{H}_2\text{O}$ , 0.63 g hexamethylenetetramine (HMT) were dissolved in 20 mL water with vigorous stirring for 30 min. Then, the mixture was transferred into a three neck flask and heated to a reflux temperature for 12 h. After cooling to room temperature naturally, the obtained products were collected by centrifugation, washed with distilled water and ethanol for several times, and dried at 60 °C in air overnight for further characterization.

### 2.3. Preparation of $V_{\text{O}}$ -rich/ $V_{\text{O}}$ -poor ultrathin NiO nanosheets

The  $V_{\text{O}}$ -rich ultrathin NiO nanosheets were synthesized from ultrathin Ni-based nanosheets precursors by a simple calcination reaction. In a typical experiment, the prepared precursors were directly heated at 350 °C for 7 min in air and then cooled to room temperature naturally. The obtained solid powders were collected for further characterization. The  $V_{\text{O}}$ -poor ultrathin NiO nanosheets were synthesized by the same method as described above, except that the annealing time was prolonged to 30 min.

### 2.4. Preparation of bulk NiO

In a typical process, 1 g  $\text{Ni}(\text{NO}_3)_2 \cdot 6\text{H}_2\text{O}$  was placed in the tube furnace and heated at 800 °C for 4 h in air and then cooled to room temperature. The obtained powders were bulk NiO and collected for further characterization.

### 2.5. Characterization

X-ray diffraction patterns (XRD) were recorded on Japan Rigaku D/max-rA equipped with graphite monochromatized high-intensity Cu K $\alpha$  radiation ( $\lambda = 1.54178 \text{ \AA}$ ). The field-emission scanning electron microscopy (FESEM) images were obtained by using a JEOL JSM-6700F scanning electron microscope. The transmission electron microscopy (TEM) and the corresponding high-resolution transmission electron microscopy (HRTEM) images were obtained by using a JEOL-2010 TEM at an acceleration voltage of 200 kV. X-ray photoelectron spectroscopy (XPS) valence spectra were acquired on an ESCALAB MKII X-ray photoelectron spectrometer with an excitation source of Mg K $\alpha = 1253.6 \text{ eV}$ . Nitrogen adsorption-desorption measurements were performed by using a Micromeritics ASAP 2000 system. All the gas adsorption experiments were carried out at 77 K after degassed at 200 °C for 6 h.

$H_2$  temperature programmed reduction ( $H_2$ -TPR) was carried out by

AutoChem II 2920 Analyzer (Micromeritics, USA). Typically, 100 mg of the catalyst sample was placed in a quartz-tube reactor, pretreated at 300 °C under a pure He atmosphere for 30 min. After cooling to room temperature, the gas atmosphere was switched to 5%  $H_2/\text{Ar}$ , and the reactor temperature rose at a rate of  $10 \text{ }^{\circ}\text{C min}^{-1}$  to 800 °C. The hydrogen consumption was detected by an in situ thermal conductivity detector (TCD).

$O_2$  temperature programmed desorption ( $O_2$ -TPD) was carried out in the same apparatus as used in  $H_2$ -TPR. Approximately 100 mg of the catalyst sample was placed in a quartz-tube reactor, pretreated at 300 °C under a pure He atmosphere for 30 min. After cooling to room temperature, the sample was treated by 5%  $O_2/\text{He}$  mixture gas for 1 h, and then the reactor was programmatically heated to 800 °C at the rate of  $10 \text{ }^{\circ}\text{C min}^{-1}$  to 800 °C. The desorbed oxygen species was detected by TCD.

### 2.6. Electrochemical measurements

All of the electrochemical measurements were performed in a three-electrode system at an electrochemical station (CHI660B). In a typical procedure, 4 mg of catalysts and 30  $\mu\text{L}$  of 5 wt % Nafion solutions (Sigma-Aldrich) were dispersed in 1 mL of water-isopropanol solution with volume ratio of 3:1 by sonicating for 1 h to form a homogeneous ink. Then, 5  $\mu\text{L}$  of the above dispersion (containing 20  $\mu\text{g}$  of catalyst) was loaded onto a glassy carbon electrode with a diameter of 3 mm (loading 0.285  $\text{mg cm}^{-2}$ ). Cyclic voltammetry (CV) was carried out at a scan rate of  $50 \text{ mV s}^{-1}$  in 1 M KOH + 0.5 M methanol solution using Ag/AgCl (3.3 M KCl) electrode as the reference electrode, a Pt electrode as the counter electrode, and the glassy carbon electrode with various catalysts as the working electrode. Electrochemical impedance spectroscopy (EIS) measurements of the various catalysts were measured with the above three electrode systems at 0.50 V vs Ag/AgCl in 1 M KOH + 0.5 M methanol solution. The amplitude of the applied voltage was 5 mV, and the frequency range was 100 K Hz to 0.1 Hz. Chronoamperometry (CA) was performed at 0.50 V vs Ag/AgCl in 1 M KOH + 0.5 M methanol solution to investigate the stability for MOR.

## 3. Results and discussion

### 3.1. Catalyst characterization and discussion

In this work, ultrathin NiO nanosheets rich in oxygen vacancies ( $V_{\text{O}}$ -rich ultrathin NiO nanosheets) and its counterpart poor in oxygen vacancies ( $V_{\text{O}}$ -poor ultrathin NiO nanosheets) were prepared by rapidly heating the Ni-based ultrathin nanosheets precursors in air (see details in Experimental Section), which is schematically illustrated in Fig. 1. The prepared products were recollected into powders to study the structural information by X-ray diffraction (XRD). As shown in Fig. 2a, all the diffraction peaks can be consistent with a face-centered cubic phase of NiO without any impurity (JCPDS 04-0835), indicating the  $V_{\text{O}}$ -rich ultrathin NiO nanosheet maintains its pristine crystal structure after the oxygen vacancy incorporation. Transmission electron microscopy (TEM) image in Fig. 2b clearly shows that the product possesses a sheet-like morphology with size of hundreds of nanometers and abundant pores irregularly distributed on surface. Meanwhile, the nearly transparent character to the electron beams suggests the ultrathin thickness of the as-obtained nanosheet. High-resolution transmission electron microscopy (HRTEM) has been carried out to further investigate the structure of the sample. As can be seen from the inset in Fig. 2b, distinct crystal fringes with interlayer distance of about  $2.4 \text{ \AA}$  can be indexed to the (111) lattice plane of face-centered cubic NiO, which is consistent with the aforementioned XRD results. In addition, Fig. S2 and Fig. S10 reveal that ultrathin NiO nanosheets poor in oxygen vacancies not only possess the same morphological and structural features, but also show almost the same specific surface area and pore size distribution as the sample rich in oxygen vacancies.

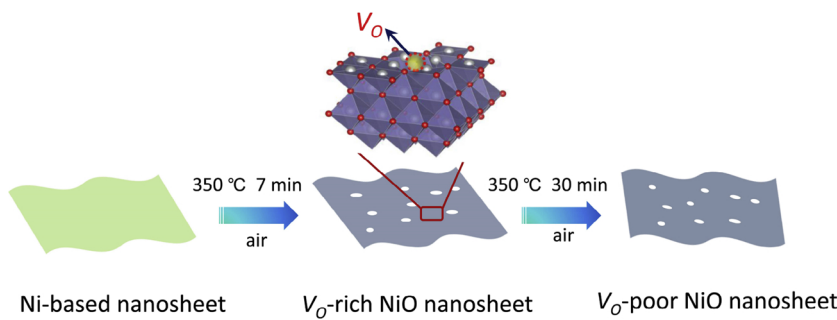


Fig. 1. Schematic illustration for the fabrication of  $V_o$ -rich/poor ultrathin NiO nanosheets.

Accordingly, these results undoubtedly demonstrate that ultrathin NiO nanosheets with porous structure have been successfully synthesized.

To go further, bulk NiO sample was also synthesized as a reference catalyst to shed light on the contribution of ultrathin nanosheet morphology during the MOR process. The chemical state and surface compositions of the  $V_o$ -rich and  $V_o$ -poor ultrathin NiO nanosheets as well as bulk NiO were investigated by X-ray photoelectron spectroscopy (XPS). The survey XPS spectrum clearly reveals that only Ni and O elements can be detected in all samples. The Ni 2p core level spectra in Fig. 2c show two major peaks located at 855.4 eV and 872.4 eV, which can be attributed to the Ni 2p<sub>3/2</sub> and 2p<sub>1/2</sub>, respectively, and the other two peaks located at 860.8 eV and 879.5 eV are their corresponding shakeup satellites. These features are in good agreement with the characteristics of the Ni<sup>2+</sup> oxidation state [21,22]. Furthermore, there are three peaks can also be clearly identified in the O 1s core level spectra. In detail, the peak at 529.7 eV and 532.6 eV are respectively attributed to the lattice oxygen of NiO and adsorbed water [19,20], while the peak at 531.4 eV is associated with the existence of oxygen vacancies in the matrix of metal oxide [23,24]. Of note, the integral area of the peak at 531.4 eV for the  $V_o$ -rich ultrathin NiO nanosheets is obviously larger than that for the  $V_o$ -poor ultrathin NiO nanosheets and

bulk NiO, which reveals that the  $V_o$ -rich ultrathin NiO nanosheets possess the highest oxygen vacancies concentration among the three samples.

### 3.2. $H_2$ -TPR and $O_2$ -TPD analysis

To investigate the reducibility of as-prepared catalysts,  $H_2$  temperature programmed reduction ( $H_2$ -TPR) was carried out on  $V_o$ -rich ultrathin NiO nanosheets and  $V_o$ -poor ultrathin NiO nanosheets and the results were displayed in Fig. 3a. For each sample, only one asymmetrical reduction peak in the range of 200–500 °C can be clearly observed, which implies the reduction processes of  $Ni^{3+}$  to  $Ni^{2+}$  and  $Ni^{2+}$  to  $Ni^{\circ}$  as previously reported in other publications [25,26]. Obviously, the reduction process of the  $V_o$ -rich ultrathin NiO nanosheets can occur at lower temperature, indicating that the  $V_o$ -rich ultrathin NiO nanosheets are much more reducible than the  $V_o$ -poor ultrathin NiO nanosheets. The difference in reduction temperature of these samples is mainly attributed to the presence of oxygen vacancy since oxygen vacancies have been proved to be favorable for oxygen diffusion [27,28]. It is well known that reduction process is closely related to the active oxygen species of catalysts, so that more available reactive oxygen

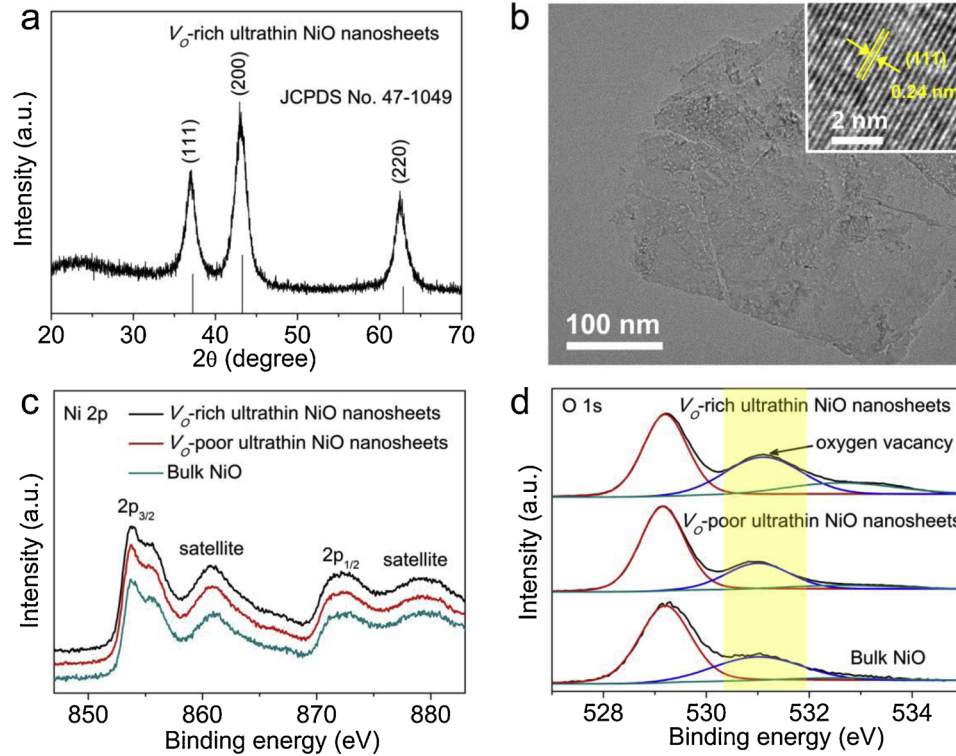
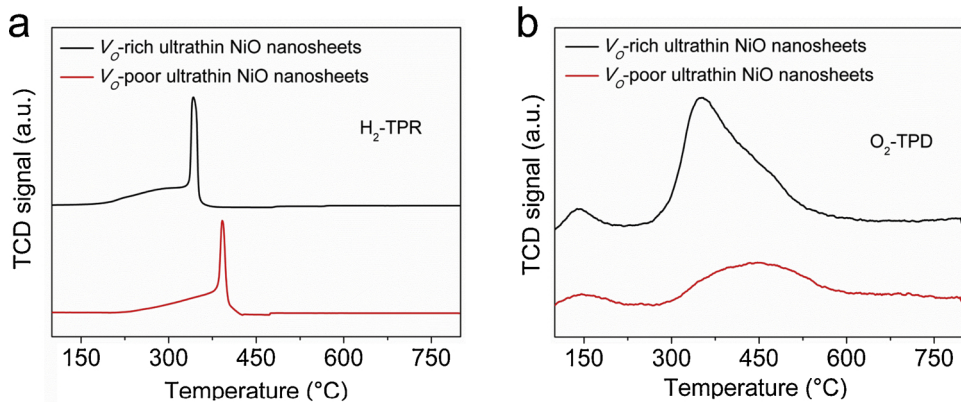


Fig. 2. (a) XRD pattern of the as-obtained  $V_o$ -rich ultrathin NiO nanosheets. (b) TEM image of a freestanding ultrathin NiO nanosheet and the corresponding HRTEM image (inset). (c) The Ni 2p spectra and (d) O 1s spectra for  $V_o$ -rich,  $V_o$ -poor ultrathin NiO nanosheets and bulk NiO.



**Fig. 3.** (a) H<sub>2</sub>-TPR profiles and (b) O<sub>2</sub>-TPD profiles of the as-prepared V<sub>O</sub>-rich ultrathin NiO nanosheets and V<sub>O</sub>-poor ultrathin NiO nanosheets.

species on the surface of V<sub>O</sub>-rich ultrathin NiO nanosheets can be directly used during the catalytic reaction, helping to improve their electrocatalytic MOR performances [29].

O<sub>2</sub> temperature programmed desorption (O<sub>2</sub>-TPD) was performed to further investigate the mobility of oxygen species on the catalysts. As shown in Fig. 3b, three kinds of oxygen desorption peaks can be observed for V<sub>O</sub>-rich ultrathin NiO nanosheets and V<sub>O</sub>-poor ultrathin NiO nanosheets samples. In detail, the peak around 150 °C denoted α oxygen (O<sub>α</sub>) is assigned to the chemisorbed oxygen O<sup>2-</sup> on the surface of NiO sample. The peaks in the region of 200–500 °C denoted β oxygen (O<sub>β</sub>) are attributed to the nonstoichiometric oxygen species of active oxygen O<sub>2</sub><sup>2-</sup>, and the peak above 500 °C denoted γ oxygen (O<sub>γ</sub>) is ascribed to the desorption of NiO lattice oxygen [30,31]. It should be noted that the peaks associated with O<sub>β</sub> and O<sub>γ</sub> for V<sub>O</sub>-rich ultrathin NiO nanosheets shift to lower desorption temperatures in comparison with the V<sub>O</sub>-poor ultrathin NiO nanosheets, demonstrating a higher oxygen migration in V<sub>O</sub>-rich ultrathin NiO nanosheets, which can be attributed to the higher concentration of newly produced oxygen vacancies and surface O<sup>2-</sup> ions. In addition, all of the peaks for V<sub>O</sub>-rich ultrathin NiO nanosheets are apparently larger than the corresponding peaks for V<sub>O</sub>-poor ultrathin NiO nanosheets, substantiating its enhanced oxygen adsorption and storage capacity, beneficial for oxidation reactions during the electrocatalytic MOR process [32,33].

### 3.3. Evaluation of electrocatalytic activity

To evaluate the electrocatalytic activity of V<sub>O</sub>-rich, V<sub>O</sub>-poor ultrathin NiO nanosheets and bulk NiO samples, a series of electrochemical measurements were carried out in a three-electrode system. Cyclic voltammetry (CV) curves of different NiO samples measured in 1 M KOH solution exhibit a pair of redox peaks between 280 and 500 mV, corresponding to the Ni<sup>2+</sup>/Ni<sup>3+</sup> redox couple [34,35]. And the linear relationships between the anodic peak current densities (I<sub>pa</sub>) and the square roots of scan rate ( $v^{1/2}$ ) can be observed in Fig. 4a. The slopes of these plots for V<sub>O</sub>-rich, V<sub>O</sub>-poor ultrathin NiO nanosheets and bulk NiO are calculated to be 1.5967, 0.5236 and 0.1221, respectively. The larger slope value for V<sub>O</sub>-rich ultrathin NiO nanosheets reveals that OH<sup>-</sup> has a better diffusion capacity on the catalyst than that on others, which is beneficial to the formation of electroactive species NiOOH on the catalyst surface, thus offering more active sites for methanol oxidation [36,37]. To further investigate the effect of oxygen vacancies on MOR, the CV curves of different NiO samples were recorded at a scan rate of 50 mV s<sup>-1</sup> with and without 0.5 M methanol in 1 M KOH solution (Figs. 4b and S6). Of note, the anodic current density increases sharply after the addition of methanol, undoubtedly revealing the high electrochemical response of V<sub>O</sub>-rich ultrathin NiO nanosheets for methanol oxidation. Moreover, as depicted in Fig. 4c, both the V<sub>O</sub>-rich and V<sub>O</sub>-poor ultrathin NiO nanosheets exhibit higher electrocatalytic MOR

activity, with larger anodic current density than that of the bulk sample. This is mainly because of the ultrathin and porous morphology of ultrathin NiO nanosheets, which can not only provide more exposed interior atoms as active sites to promote the electro-oxidation of methanol, but also endow with easier electrolyte infiltration and larger contact area with the electrolyte to enlarge the reaction space for MOR with respect to the bulk sample. In detail, V<sub>O</sub>-rich ultrathin NiO nanosheets possess a large anodic current density of 85.3 mA cm<sup>-2</sup> at 0.7 V vs. Ag/AgCl, which is about 2.3 times and 3.5 times higher than the value of V<sub>O</sub>-poor ultrathin NiO nanosheets (36.9 mA cm<sup>-2</sup>) and bulk NiO (23.9 mA cm<sup>-2</sup>), respectively, verifying the positive effect of the oxygen vacancies on the MOR process. Of note, compared to the commercial Pt/C (5 wt%) and some other Ni-based catalysts, V<sub>O</sub>-rich ultrathin NiO nanosheets also exhibit a much higher current density at the same conditions, further demonstrating its superior electrocatalytic performance for MOR.

The MOR catalytic kinetics of different catalysts was further evidenced by the linear sweep voltammetry curves and corresponding Tafel plots. As can be seen from Fig. 4d, Tafel slope of V<sub>O</sub>-rich ultrathin NiO nanosheets is calculated to be about 42 decade<sup>-1</sup>, smaller than that of V<sub>O</sub>-poor ultrathin NiO nanosheets (80 mV decade<sup>-1</sup>) and bulk NiO (111 mV decade<sup>-1</sup>), which demonstrates its significantly improved reaction kinetics for MOR. Furthermore, electrochemical impedance spectroscopy (EIS) in Fig. 4e reveals that V<sub>O</sub>-rich ultrathin NiO nanosheets have the lowest interfacial charge-transfer resistance in comparison to the other two samples, indicating its superior charge transport kinetics during the MOR process. Apart from the catalytic activity, the catalytic stability is another crucial factor to evaluate a dependable electrocatalyst for methanol oxidation. As depicted in Fig. 4f, the chronoamperometric measure was conducted in 1 M KOH solution containing 0.5 M methanol at 0.5 V vs. Ag/AgCl for a duration of 30,000 s. The average current density of V<sub>O</sub>-rich ultrathin NiO nanosheets for methanol oxidation is obviously higher than that of two other samples, and negligible drops in the anodic current density can be observed even after a long period of tests, clearly revealing the excellent catalytic stability of V<sub>O</sub>-rich ultrathin NiO nanosheets for MOR, which favors long-term application as an excellent anode material in fuel cells. In addition, TEM image of V<sub>O</sub>-rich ultrathin NiO nanosheets after the chronoamperometric test further confirms its excellent structural stability under alkaline conditions, and no apparent morphology change can be identified during the electrocatalytic process.

### 3.4. Theoretical calculations for investigating the effect of oxygen vacancy on the improvement of electrocatalytic performance

It is well known that electrical conductivity play a crucial role in electrocatalytic process, which is determined by the electronic structures of catalyst materials [38]. Taking models of NiO samples with and

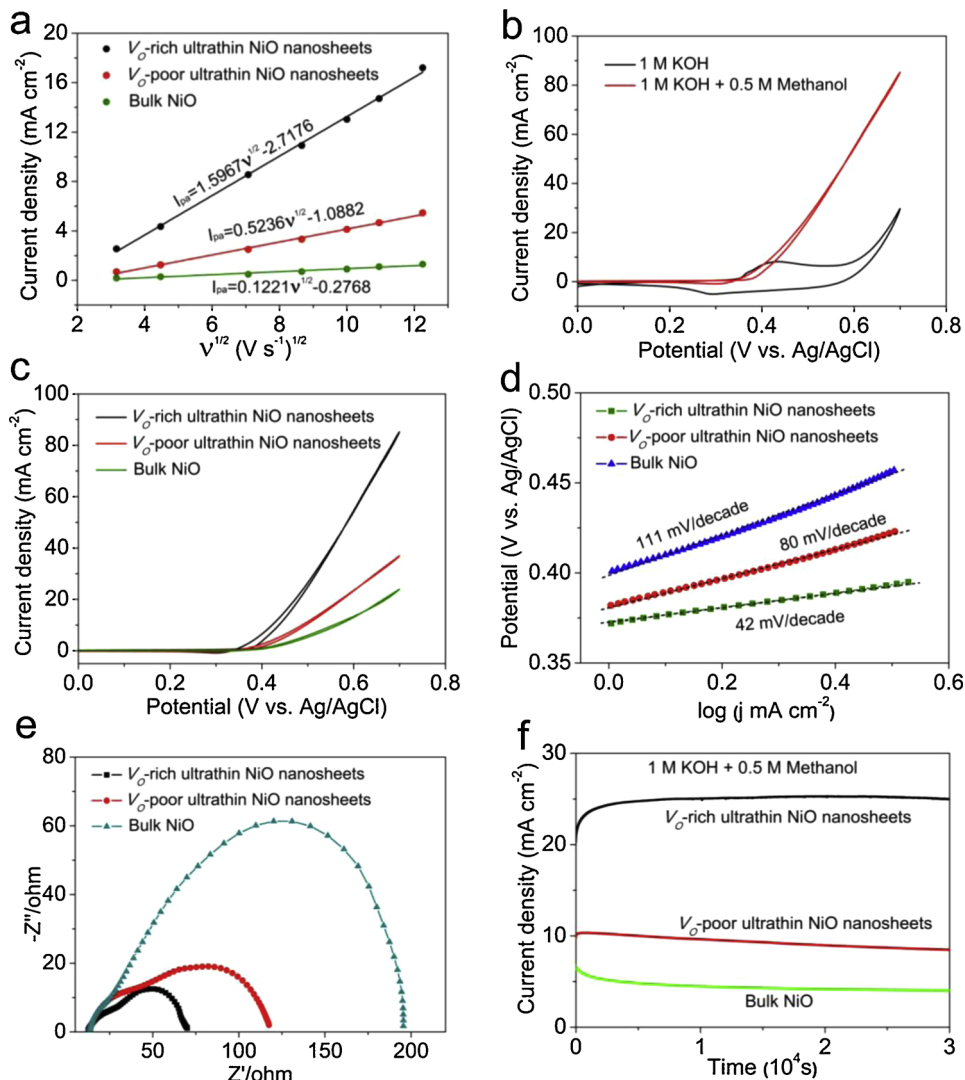


**Fig. 4.** (a) Linear relationship between the anodic peak current and the square root of the scan rate ( $I_{pa} \sim V^{1/2}$ ) in 1 M KOH solution. (b) Cyclic voltammetry (CV) curves of  $V_o$ -rich ultrathin NiO nanosheets in 1 M KOH solution at a scan rate of  $50 \text{ mV s}^{-1}$  with and without 0.5 M methanol. (c) CV curves, (d) Tafel plots and (e) Electrochemical impedance spectra of various NiO samples in 1 M KOH solution with 0.5 M methanol. (f) Chronoamperograms of various NiO samples in 1 M KOH solution with 0.5 M methanol at the potential of 0.5 V vs. Ag/AgCl.

without oxygen vacancies as examples, first principle calculations based on density functional theory (DFT) were implemented to investigate the influence of oxygen vacancies on the electronic structure and properties of NiO catalyst. As disclosed by the calculated density of states (DOS) in Fig. 5a and b,  $V_o$ -NiO shows a smaller band gap of 1.08 eV with respective to the pristine NiO (1.6 eV). Evidently, the introduction of oxygen vacancies endows the NiO catalyst with a new defect level, which serves as the springboard for electronic transition from valence band to conduction band. It is greatly conducive to the excitation of electrons into the conduction band, thereby achieving enhanced electron transport capacity and superior MOR performance. Generally, the adsorption energy of methanol molecules onto the active sites is regarded as another important factor in affecting the MOR activity, since methanol molecules are initially adsorbed onto the surface of the catalyst during the MOR process [39]. As can be observed from the deformation charge density of NiO catalyst with oxygen vacancy (Fig. 5c), the electrons neighboring the oxygen vacancy that previously occupied oxygen 2p orbital become delocalized, suggesting a much higher degree of electron delocalization in the surface with oxygen vacancy. Owing to the high degree of electron delocalization, the  $\text{Ni}^{2+}$  near the oxygen vacancy will be in an activated state, which is more active for the adsorption of oxygen-containing ligands, such as methanol molecule, to

form the six-coordinated structure than that for  $\text{Ni}^{2+}$  in the surface without oxygen vacancy. Furthermore, the existence of oxygen vacancy could also decrease the coordination number of Ni atoms, which benefits the adsorption of methanol molecules onto the surface of NiO catalyst, since low-coordinated surface possessed extremely high amount of active sites and better catalytic activity [40]. In that case, methanol molecules would be preferentially adsorbed on the surface with oxygen vacancies to reduce their adsorption energy. Notably, a significant charge transfer between methanol molecules and Ni atoms near the oxygen vacancy can indeed occur with the methanol molecule adsorbed on the surface of NiO, demonstrating that the charged Ni ions at surface will serve as active sites with high reactivity toward methanol oxidation. Moreover, the hindrance for the adsorption of methanol molecules on the NiO catalyst surface obviously decreases with the incorporation of oxygen vacancies. As shown in Fig. 5d, the adsorption energy for NiO surface with oxygen vacancies is calculated to be -5.81 eV, lower than that of the perfect surface (-3.57 eV), which indicates that the presence of oxygen vacancies can promote the adsorption of methanol molecules onto the surface of NiO catalyst, thus accelerating the sluggish catalytic kinetics for MOR.

On the basis of these results, the significantly enhanced MOR performance of  $V_o$ -rich ultrathin NiO nanosheets can be attributed to the

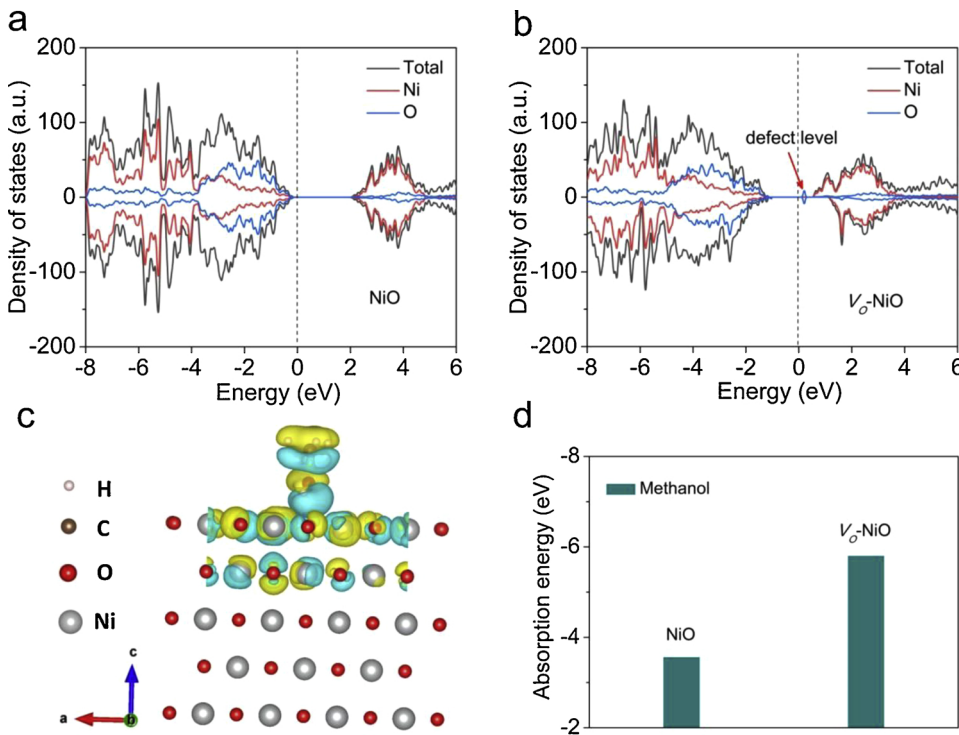


**Fig. 5.** Calculated density of states (DOS) of NiO samples without (a) and with (b) oxygen vacancy. (c) Illustration of the adsorption of methanol molecules onto the surface of  $V_o$ -NiO sample and the deformation charge density of NiO with oxygen vacancy. (d) Adsorption energy of methanol molecules on the NiO and  $V_o$ -NiO samples.

synergistic effect between the macroscopic morphological characteristics and microscopic structural features. In detail, the ultrathin thickness of NiO nanosheets enables a larger surface active area with respect to the bulk counterpart, guaranteeing abundant active sites to promote the surface reaction. Furthermore, the presence of oxygen vacancies can significantly modify the electronic structure of ultrathin NiO nanosheets, which can not only facilitate the electron transport along the 2D conducting channels, but also reduce the energy required for the adsorption of methanol molecules onto the surface of catalyst, leading to a remarkable improvement in the MOR reaction kinetics. In addition, the ultrathin 2D structure brings an intimate contact with the substrate electrode and a large interfacial contact area with the electrolyte as well as shorter ion diffusion paths to expedite the rate of electrochemical reaction.

#### 4. Conclusions

In summary, the structurally-new  $V_o$ -rich ultrathin NiO nanosheets have been successfully constructed and employed as an excellent platform to promote the electrocatalytic MOR activity through a facile defect engineering strategy. Taking the advantages of ultrathin 2D structure and abundant oxygen vacancies, the obtained  $V_o$ -rich ultrathin NiO nanosheets showed a stable and remarkably increased MOR activity with a current density up to  $85.3 \text{ mA cm}^{-2}$  at  $0.7 \text{ V}$  vs. Ag/AgCl, which is roughly 2.3 times and 3.5 times larger than that of the  $V_o$ -poor ultrathin NiO nanosheets and bulk NiO samples, respectively. DFT calculations disclosed that the introduction of oxygen vacancies endows the NiO catalyst with an additional defect state, ensuring a faster charge transfer during the MOR process. Furthermore, the calculated adsorption energy confirmed the importance of oxygen vacancies in facilitating the adsorption of methanol molecules on the surface of NiO catalyst, thereby resulting in the significantly improved MOR kinetics. By combining theoretical calculations with experimental studies, this work not only sheds light on the crucial role of oxygen vacancy in promoting electrocatalytic activity at the atomic level, but also provides a feasible pathway for the design of advanced electrocatalysts with stable performance for MOR.

#### Acknowledgements

This work was supported by the National Natural Science Foundation of China (21675093, 21805149, 41573103, 21422504), the Natural Science Foundation of Shandong Province of China (ZR2018BB012, 2015ZRB01A0D), and the Taishan Scholar Program of Shandong Province of China (ts20110829).

#### References

- [1] N. Kakati, J. Maiti, S.H. Lee, S.H. Jee, B. Viswanathan, Y.S. Yoon, Anode catalysts for direct methanol fuel cells in acidic media: do we have any alternative for Pt or Pt-Ru, *Chem. Rev.* 114 (2014) 12397–12429.
- [2] C. Bianchini, P.K. Shen, Palladium-based electrocatalysts for alcohol oxidation in half cells and in direct alcohol fuel cells, *Chem. Rev.* 109 (2009) 4183–4206.
- [3] W. Li, Y. Bai, F. Li, C. Liu, K.Y. Chan, X. Feng, X. Lu, Core-shell  $\text{TiO}_2/\text{C}$  nanofibers as supports for electrocatalytic and synergistic photoelectrocatalytic oxidation of methanol, *J. Mater. Chem.* 22 (2012) 4025–4031.
- [4] Z. Wu, Y. Lv, Y. Xia, P.A. Webley, D. Zhao, Ordered mesoporous Platinum@Graphitic carbon embedded nanophasse as a highly active, stable, and methanol-tolerant oxygen reduction electrocatalyst, *J. Am. Chem. Soc.* 134 (2012) 2236–2245.
- [5] H.J. Qiu, X. Shen, J.Q. Wang, A. Hirata, T. Fujita, Y. Wang, M.W. Chen, Aligned nanoporous Pt-Cu bimetallic microwires with high catalytic activity toward methanol electrooxidation, *ACS Catal.* 5 (2015) 3779–3785.
- [6] X.H. Sun, K.Z. Jiang, N. Zhang, S.J. Guo, X.Q. Huang, Crystalline control of {111} bounded Pt<sub>3</sub>Cu nanocrystals: multiply-twinned Pt<sub>3</sub>Cu icosahedra with enhanced electrocatalytic properties, *ACS Nano* 9 (2015) 7634–7640.
- [7] F.S. Hoor, C.N. Tharamani, M.F. Ahmed, S.M. Mayanna, Electrochemical synthesis of Fe-Mo and Fe-Mo-Pt alloys and their electrocatalytic activity for methanol oxidation, *J. Power Sources* 167 (2007) 18–24.
- [8] A.B.A.A. Nassr, I. Sinev, M.M. Pohl, W. Grünert, M. Bron, Rapid microwave-assisted polyol reduction for the preparation of highly active PtNi/CNT electrocatalysts for methanol oxidation, *ACS Catal.* 4 (2014) 2449–2462.
- [9] E. Antolini, E.R. Gonzalez, Alkaline direct alcohol fuel cells, *J. Power Sources* 195 (2010) 3431–3450.
- [10] L. Qian, L. Gu, L. Yang, H.Y. Yuan, D. Xiao, Direct growth of  $\text{NiCo}_2\text{O}_4$  nanostructures on conductive substrates with enhanced electrocatalytic activity and stability for methanol oxidation, *Nanoscale* 5 (2013) 7388–7396.
- [11] Y.S. Xia, H.X. Dai, H.Y. Jiang, L. Zhang, Three-dimensional ordered mesoporous cobalt oxides: highly active catalysts for the oxidation of toluene and methanol, *Catal. Commun.* 11 (2010) 1171–1175.
- [12] J.B. Wu, Z.G. Li, X.H. Huang, Y. Lin, Porous  $\text{Co}_3\text{O}_4/\text{NiO}$  core/shell nanowire array with enhanced catalytic activity for methanol electro-oxidation, *J. Power Sources* 224 (2013) 1–5.
- [13] L.Y. Wang, G.G. Zhang, Y. Liu, W.F. Li, W. Lu, H.T. Huang, Facile synthesis of a

- mechanically robust and highly porous NiO film with excellent electrocatalytic activity towards methanol oxidation, *Nanoscale* 8 (2016) 11256–11263.
- [14] J. Wang, D. Teschner, Y.Y. Yao, X. Huang, M. Willinger, L.D. Shao, R. Schlogl, Fabrication of nanoscale NiO/Ni heterostructures as electrocatalysts for efficient methanol oxidation, *J. Mater. Chem. A* 5 (2017) 9946–9951.
- [15] X.L. Tong, Y. Qin, X.Y. Guo, O. Moutanabbir, X.Y. Ao, E. Pippel, L.B. Zhang, M. Knez, Enhanced catalytic activity for methanol electro-oxidation of uniformly dispersed nickel oxide nanoparticles-carbon nanotube hybrid materials, *Small* 8 (2012) 3390–3395.
- [16] M.U.A. Prathap, B. Satpati, R. Srivastava, Facile preparation of  $\beta$ -Ni(OH)<sub>2</sub>-NiCo<sub>2</sub>O<sub>4</sub> hybrid nanostructure and its application in the electro-catalytic oxidation of methanol, *Electrochim. Acta* 130 (2014) 368–380.
- [17] Y.F. Sun, S. Gao, F.C. Lei, C. Xiao, Y. Xie, Ultrathin two-dimensional inorganic materials: new opportunities for solid state nanochemistry, *Acc. Chem. Res.* 48 (2015) 3–12.
- [18] W.L. Yang, X.D. Zhang, Y. Xie, Advances and challenges in chemistry of two-dimensional nanosheets, *Nano Today* 11 (2016) 793–816.
- [19] J. Bao, X.D. Zhang, B. Fan, J.J. Zhang, M. Zhou, W.L. Yang, X. Hu, H. Wang, B.C. Pan, Y. Xie, Ultrathin spinel-structured nanosheets rich in oxygen deficiencies for enhanced electrocatalytic water oxidation, *Angew. Chem. Int. Ed.* 54 (2015) 7507–7512.
- [20] Y. Tong, P.Z. Chen, M.X. Zhang, T.P. Zhou, L.D. Zhang, W.S. Chu, C.Z. Wu, Y. Xie, Oxygen vacancies confined in nickel molybdenum oxide porous nanosheets for promoted electrocatalytic urea oxidation, *ACS Catal.* 8 (2018) 1–7.
- [21] X.J. Zhu, X.Y. Dou, J. Dai, X.D. An, Y.Q. Guo, L.D. Zhang, S. Tao, J.Y. Zhao, W.S. Chu, X.C. Zeng, C.Z. Wu, Y. Xie, Metallic nickel hydroxide nanosheets give superior electrocatalytic oxidation of urea for fuel cells, *Angew. Chem. Int. Ed.* 55 (2016) 12465–12469.
- [22] D.D. Zhu, C.X. Guo, J.L. Liu, L. Wang, Y. Du, S.Z. Qiao, Two-dimensional metal-organic frameworks with high oxidation states for efficient electrocatalytic urea oxidation, *Chem. Commun.* 53 (2017) 10906–10909.
- [23] L. Xu, Q.Q. Jiang, Z.H. Xiao, X.Y. Li, J. Huo, S.Y. Wang, L.M. Dai, Plasma-engraved Co<sub>3</sub>O<sub>4</sub> nanosheets with oxygen vacancies and high surface area for the oxygen evolution reaction, *Angew. Chem. Int. Ed.* 55 (2016) 5277–5281.
- [24] L.J. Li, J. Zhang, J.L. Lei, J. Xu, B. Shang, L. Liu, N.B. Li, F.S. Pan, O-vacancy-Enriched NiO hexagonal platelets fabricated on Ni foam as a self-supported electrode for extraordinary pseudocapacitance, *J. Mater. Chem. A* 6 (2018) 7099–7106.
- [25] Y.Z. Deng, W.X. Tang, W.H. Li, Y.F. Chen, MnO<sub>2</sub>-nanowire@NiO-nanosheet core-shell hybrid nanostructure derived interfacial effect for promoting catalytic oxidation activity, *Catal. Today* 308 (2018) 58–63.
- [26] G.M. Bai, H.X. Dai, J.G. Deng, Y.X. Liu, K.M. Ji, Porous NiO nanoflowers and nanoribbons: highly active catalysts for toluene combustion, *Catal. Commun.* 27 (2012) 148–153.
- [27] X.W. Liu, K.B. Zhou, L. Wang, B.Y. Wang, Y.D. Li, Oxygen vacancy clusters promoting reducibility and activity of Ceria nanorods, *J. Am. Chem. Soc.* 131 (2009) 3140–3141.
- [28] K.Y. Ahn, D.S. Yoo, D.H. Prasad, H.W. Lee, Y.C. Chung, J.H. Lee, Role of multivalent Pr in the formation and migration of oxygen vacancy in Pr-doped Ceria: experimental and first-principles investigations, *Chem. Mater.* 24 (2012) 4261–4267.
- [29] W.X. Tang, Y.Z. Deng, W.H. Li, S.D. Li, X.F. Wu, Y.F. Chen, Restrictive nanoreactor for growth of transition metal oxides (MnO<sub>2</sub>, Co<sub>3</sub>O<sub>4</sub>, NiO) nanocrystal with enhanced catalytic oxidation activity, *Catal. Commun.* 72 (2015) 165–169.
- [30] J.H. Li, C.C. Wang, C.J. Huang, Y.F. Sun, W.Z. Weng, H.L. Wan, Mesoporous nickel oxides as effective catalysts for oxidative dehydrogenation of propane to propene, *Appl. Catal. A* 382 (2010) 99–105.
- [31] X.L. Xu, L. Li, J. Huang, H. Jin, X.Z. Fang, W.M. Liu, N. Zhang, H.M. Wang, X. Wang, Engineering Ni<sup>3+</sup> Cations in NiO Lattice at the Atomic Level by Li<sup>+</sup> Doping: The Roles of Ni<sup>3+</sup> and Oxygen Species for CO Oxidation, *ACS Catal.* 8 (2018) 8033–8045.
- [32] G.F. Zhao, J. Huang, Z. Jiang, S. Zhang, L. Chen, Y. Lu, Microstructured Au/Ni-Fiber catalyst for low-temperature gas-phase alcohol oxidation: evidence of Ni<sub>2</sub>O<sub>3</sub>-Au<sup>+</sup> hybrid active sites, *Appl. Catal. B* 140 (2013) 249–257.
- [33] Q. Wang, L.F. Chen, S.L. Guan, X. Zhang, B. Wang, X.Z. Cao, Z. Yu, Y.F. He, D.G. Evans, J.T. Feng, D.Q. Li, Ultrathin and vacancy-rich CoAl-Layered double Hydroxide/Graphite oxide catalysts: promotional effect of cobalt vacancies and oxygen vacancies in alcohol oxidation, *ACS Catal.* 8 (2018) 3104–3115.
- [34] A. Pintar, J. Batista, Improvement of an integrated ion-exchange/catalytic process for nitrate removal by introducing a two-stage denitrification step, *Appl. Catal. B* 63 (2006) 150–159.
- [35] H.L. Wang, H.S. Casalongue, Y.Y. Liang, H.J. Dai, Ni(OH)<sub>2</sub> nanoplates grown on graphene as advanced electrochemical pseudocapacitor materials, *J. Am. Chem. Soc.* 132 (2010) 7472–7477.
- [36] S. Xie, X.L. Tong, G.Q. Jin, Y. Qin, X.Y. Guo, CNT-Ni/SiC hierarchical nanostructures: preparation and their application in electrocatalytic oxidation of methanol, *J. Mater. Chem. A* 1 (2013) 2104–2109.
- [37] M.S. Kim, T.S. Hwang, K.B. Kim, A study of the electrochemical redox behavior of electrochemically precipitated nickel hydroxides using electrochemical quartz crystal microbalance, *J. Electrochem. Soc.* 144 (1997) 1537–1543.
- [38] Y.F. Sun, S. Gao, F.C. Lei, Y. Xie, Atomically-thin two-dimensional sheets for understanding active sites in catalysis, *Chem. Soc. Rev.* 44 (2015) 623–636.
- [39] X. Gui, P. Xiao, J. Wang, M. Zhou, W.L. Guo, Y. Yang, Y.J. He, Z.W. Wang, Y.K. Yang, Y.H. Zhang, Z.Q. Lin, Highly branched metal alloy networks with superior activities for the methanol oxidation reaction, *Angew. Chem. Int. Ed.* 56 (2017) 4488–4493.
- [40] Y.F. Sun, F.C. Lei, S. Gao, B.C. Pan, J.F. Zhou, Y. Xie, Atomically thin tin dioxide sheets for efficient catalytic oxidation of carbon monoxide, *Angew. Chem. Int. Ed.* 52 (2013) 10569–10572.